1995

# Compressibility Effects on Dynamic Stall of Oscillating Airfoils

Chandrasekhara, M.S.

Paper presented at the AGARD FDP Symposium on "Aerodynamics and Aeroacoustics of Rotorcraft" held in Berlin, Germany from 10-13 October 1994 and published in CP-552.

# Compressibility Effects on Dynamic Stall of Oscillating Airfoils

M.S. Chandrasekhara[1]
Associate Director and Research Associate Professor
Navy-NASA Joint Institute of Aeronautics
Department of Aeronautics and Astronautics
Naval Postgraduate School, Monterey, CA 93943

and

L.W. Carr
Research Scientist and Group Leader, Unsteady Viscous Flows
Aeroflightdynamics Directorate, U.S.Army ATCOM and,
Fluid Mechanics Laboratory Branch
NASA Ames Research Center, Moffett Field, CA 94035-1000, U.S.A.

## 1. SUMMARY

A review of experimental results from an ongoing study of the effects of compressibility on dynamic stall of an oscillating NACA 0012 airfoil is presented. The study shows that compressibility effects become significant at a free stream Mach number of 0.3. Dynamic stall is accelerated above this Mach number, but increasing unsteadiness delays onset of stall even under compressible flow conditions. Interferometric images of the flow show that process of dynamic stall occurs rapidly over a small angle of attack range. For certain flow conditions, multiple shocks form in the flow near the airfoil leading edge. The delay of stall has been shown to be due to delayed development combined with modification of the adverse pressure gradient in the flow. Transition has been shown to significantly modify the observed flow behavior, and thus is a very important factor to be considered, especially since it occurs near the vortex formation location. Proper modelling of its effects is critical in dynamic stall flow computations.

## LIST OF SYMBOLS

| | |
|---|---|
| $C_p$ | pressure coefficient |
| $C_{p_{min}}$ | peak suction pressure coefficient |
| c | airfoil chord |
| f | frequency of oscillation, Hz |
| k | reduced frequency $= \frac{\pi f c}{U_\infty}$ |
| M | free stream Mach number |
| $U_\infty$ | free stream velocity |
| x,y | chordwise and vertical distance |
| $\alpha$ | angle of attack |
| $\alpha_0$ | mean angle of attack |
| $\alpha_m$ | amplitude of oscillation |
| $\omega$ | circular frequency, radians/sec |

## 2. INTRODUCTION

The performance of a helicopter is severely restricted by the occurrence of dynamic stall on its retreating blade; it is critical to avoid the consequent concomitant strong pitching moment variations that are destructive to the vehicle. The retreating blade operates in a strongly compressible environment at a high Reynolds number and its stall is a clear case of forced, large amplitude, unsteady, flow separation. A characteristic feature of the flow is the formation of the dynamic stall vortex due to the coalescence of the vorticity input by the unsteady pitching motion. The leading edge favorable pressure gradient in the flow is $O(10^2 - 10^3)$ and thus, the fluid encounters a region of strong adverse pressure gradient immediately following the suction peak, which could by itself cause flow separation. The large flow acceleration can induce supersonic velocities near the leading edge. In fact, it has been shown (Ref. 1) that compressibility effects appear in the flow at a very low free stream Mach number of 0.2. Many airfoils show a dramatic change in the stall behavior under this condition, as the normal trailing-edge stall becomes leading-edge stall. The dynamic stall vortex still forms, now in the presence of strongly compressible flow. Shocks can form in the flow and interact with the airfoil boundary layer, possibly inducing premature flow separation, and leading to early formation of a dynamic stall vortex. Thus, dynamic stall onset can occur from a completely different mechanism than that observed from low speed experiments. The complexity of the fluid mechanics issues of dynamic stall flow have defied a proper and thorough understanding of the fundamental aspects of the process (Ref. 2 and 3). To this series of issues needs to be added factors like the effects of transition of the boundary layer (or shear layer), and the effects of Reynolds number on the state of turbulence in the boundary layer under compressible flow conditions. In almost all cases, dynamic stall occurs as leading edge stall near the location where the flow undergoes transition, even when the chord based Reynolds number is in the turbulent regime. The transition point moves upstream with increasing angle of attack, and the transition length decreases with the increasing adverse pressure gradient(Ref. 4) as the airfoil is pitched up. This ever changing transition behavior immensely complicates the flow physics, and its proper physical modelling is a major requirement for the study. Much of the disagreement between experimental data and computational results can be attributed to improper physical modelling of the effects of transition, and the role transition plays in the dynamic stall process. However, since the relevant physics still eludes researchers, one is forced to make poor approximations to represent the flow, such as turbulence models based on equilibrium turbulent flow.

[1] **Mailing Address: M.S. 260-1, NASA Ames Research Center, Moffett Field, CA 94035-1000, U.S.A.**

*Paper presented at the AGARD FDP Symposium on "Aerodynamics and Aeroacoustics of Rotorcraft" held in Berlin, Germany from 10-13 October 1994 and published in CP-552.*

An important connection between laboratory experiments and full scale testing occurs through model rotor testing. Laboratory tests are generally performed in 2-D flow due to their lesser degree of complexity and questions have arisen concerning the applicability of 2-D tests to the complex helicopter flow environment. But, it is worth noting that in a recent workshop on three dimensional oscillatory dynamic stall(Ref. 5), it was concluded that two dimensional dynamic stall tests gave acceptable lift, drag and moment distributions for calibrating three dimensional computational codes, except very near the wing tip. The consensus of the participants was that the critical difficulty was in fact in accurately predicting two dimensional dynamic stall. In a recent attempt to extend model rotor test data to full scale rotors, the boundary layer was tripped and tests were conducted(Ref. 6). However, tripping an airfoil is a formidable task(Ref. 7) especially since the trip location nearly coincides with the vortex origination point and the consequences of the presence of a trip in this sensitive compressible flow region are not easy to separate.

The present studies are specifically aimed at understanding the underlying processes of dynamic stall, under compressible transitional flow conditions; the previous studies (Ref. 8 and 9) mainly concerned with establishing the various loads and moment loops for different airfoil shapes at high Reynolds numbers. The goal of this research is to eventually develop dynamic stall control concepts that are applicable to a practical helicopter. This paper reviews the results of the research investigation being conducted in the Navy-NASA Joint Institute of Aeronautics at NASA Ames Research Center.

## 3. EXPERIMENTAL FACILITY AND FACILITY

The experiments were conducted in the *Compressible Dynamic Stall Facility*(CDSF) which is a 25cm x 35cm test section wind tunnel with a specially designed (Ref. 10) airfoil oscillating drive system. The airfoil is supported between two optical glass windows in the CDSF. The uniqueness of the model support system provides unobstructed optical access to the complete airfoil contour, which is critical since dynamic stall events originate from the surface near the airfoil leading edge. The operating envelope of the CDSF is wider than the flight envelope of the present day helicopter. Also, the results are directly applicable to that of a $\frac{1}{7}^{th}$ scale model rotor. Fig. 1 shows the details of the facility. The airfoil angle of attack can be arbitrarily set between 0 - 15 deg., with the amplitude and frequency of oscillation continuously variable from 2 - 10 deg. and 0 - 100 Hz respectively. The tunnel Mach number can be varied from 0 - 0.5 by a choked downstream throat. The airfoil used in the tests is NACA 0012 with 7.62cm chord. The test Reynolds number ranged from $0.36 \times 10^6 - 0.81 \times 10^6$ for Mach numbers from 0.2 to 0.45.

In addition to stroboscopic schlieren flow visualization pictures, quantitative experimental data was obtained using the recently developed (Ref. 11) real time technique of point diffraction interferometry, (PDI). PDI uses an expanded laser beam to fill the entire field of view in a standard Z-type schlieren configuration, with the optics aligned to minimize astigmatism. A pre-developed, partially transmitting photographic plate replaces the knife edge. In operation, a pin-hole is created *in situ* in the photographic plate with no flow in the test section. This pin-hole serves as a point diffractor. During the wind tunnel test, the light beam passing through the flow is deflected due to density changes in the flow field and thus focuses to a bigger spot around the pin-hole. The portion of this distorted light beam passing through the pin-hole then becomes the reference beam and interferes with the portion passing around it (signal beam) to create fringes in real-time, which are captured on Polaroid film. A schematic of the PDI system is illustrated in Fig. 2. A large number of flow interferograms have been obtained and analyzed to provide a quantitative flow description. A custom interferogram image processing package has been developed for the purpose.

The experiments were performed at Mach numbers of 0.2, 0.25, 0.3, 0.35, 0.4 and 0.45. The reduced frequencies were 0(steady), 0.025, 0.05, 0.075 and 0.1. The angle of attack variation was $\alpha = 10^0 + 10^0 \sin \omega t$. Some of the important results from this experimental data base will be discussed in the next section.

## 4. RESULTS AND DISCUSSION

### 4.1. Qualitative Flow Description

#### 4.1.1. Effect of Mach Number

Figure 3 (Ref. 12) shows stroboscopic schlieren pictures of the flow over an oscillating airfoil at different Mach numbers. These pictures obtained over an exposure time of $1.5 \mu sec$ represent the instantaneous density gradient field without any history effects present, unlike most other flow visualization images. The dynamic stall vortex can be seen as a dark circular structure at approximately 50% chord location in all images with lighter shades of gray towards the leading edge (due to the orientation of the knife edge); the streaks seen slightly downstream of the vortex at x/c = 0.7 are cracks in the glass. It is interesting that the angle of attack at which the vortex reaches this location is 15.1 deg. up to M = 0.25, but as the Mach number increases, the corresponding angle decreases monotonically; for example, it is 13.8 deg. at M = 0.35, 12.7 deg. at M = 0.4 and 12.3 deg. at M = 0.45. This is photographic evidence that the angle of attack at which the dynamic stall process is initiated is independent of Mach number up to M = 0.3 and decreases with increasing Mach number beyond this value. Thus, it can be said that compressibility effects set in at M = 0.3 and premature dynamic stall occurs at higher Mach numbers.

Quantitative support to the above statement can be found in the data presented in Fig. 4, (Ref. 12). Stroboscopic schlieren pictures were obtained for a wide range of different conditions. The pictures were analyzed by following the movement of the vortex center along the airfoil upper surface. It can be seen that (within experimental scatter) up to M = 0.3, the vor-

tex trajectory as a function of the angle of attack is nearly identical. However, for $M \geq 0.3$, the curves depart considerably, moving to progressively lower angles of attack as the Mach number is increased. This supports the conclusion that the threshold for significant compressibility effects is at M = 0.3. As M is increased above 0.3, the vortex originates at lower angles of attack and is also shed at correspondingly lower angles of attack. Thus, compressibility accelerates the initiation of the dynamic stall vortex and hence, occurrence of deep stall.

**4.1.2.** Effect of Unsteadiness

Figure 5 (Ref. 13) is a plot of the dynamic stall angle of attack *vs.* reduced frequency for different Mach numbers. The results discussed above can be seen in this figure as well. It should be noted that for any given Mach number, as the reduced frequency is increased, the dynamic stall angle also increases. Thus, even though dynamic stall occurs at lower angles of attack at higher values of M, dynamic stall can be delayed by increasing the reduced frequency in the compressible flow regime as well. Thus, increasing unsteadiness always delays occurrence of stall. The reason for this is believed to be the way in which unsteadiness alters the airfoil leading edge pressure distribution (see Sec. 4.2.3) and thus, the vorticity production there.

Other noteworthy results include the fact that the vortex convection velocity was 30% of the free stream velocity for all cases studied. No shocks could be detected in the images obtained in the schlieren studies for these conditions (see Sec. 4.2.4), but a small shock was observed for the case of $\alpha = 10^0 + 2^0 \sin \omega t$ at M = 0.45 and k = 0.075, (Ref. 14).

Having identified the features of the flow after the vortex has formed, attention will now be focused on the finer details of the flow. It is worth noting that for control purposes, the game is already 'lost' once the vortex has formed.

## 4.2. Flow Description from PDI Studies

**4.2.1.** Dynamic Stall Flow Development

Figure 6 (Ref. 15) shows a sequence of interferograms obtained over the oscillating airfoil for M = 0.35 and k = 0.05. The fringes seen in it are constant density contours of the flow. The stagnation point is on the airfoil lower surface, near the leading edge and the fringes are seen to converge here. At $\alpha = 10.65^0$, (Fig. 6a) a moderately thick boundary layer is seen near the trailing edge. The fringes indicate that there is a slight local trailing edge separation; however, it appears to have no measurable effect on the overall flow. The fringes at $\alpha = 12.11^0$ (seen in Fig. 6b), after radiating from around the leading edge, turn towards the airfoil upper surface downstream of the suction peak. But, when they encounter the local boundary layer, they turn sharply again towards the trailing edge. A closer examination reveals that there is a small region on the upper surface near the leading edge which is enclosed by the fringes that physically appears like a bubble. Pressure distributions (see Ref. 16) deduced from the interferograms confirm that a laminar separation bubble is present under these conditions. As the angle of attack is increased, the bubble breaks down and a vortical structure appears at $\alpha = 12.83^0$. The static stall angle for M = 0.35 is 11.6 deg. and thus, the first indication that the dynamic stall *delay* has ended and the dynamic stall process *itself* has begun is seen in Fig. 6d, 1.2 degrees beyond static stall. The events that lead to the formation of dynamic stall vortex occur very rapidly from this angle of attack, in a very small angle of attack range, (less than one degree, shown in Fig. 6b - 6d). Thus, the complete details of the changes are not easy to capture; the rapidity of the process and possible cycle-to-cycle variations make it a very challenging measurement problem. The earlier schlieren data showed that the deep dynamic stall angle for this case was 15.2 deg.; thus, by $\alpha = 16.02^0$, deep dynamic stall has already occurred. However, the number of fringes on the lower surface near the trailing edge shows that sharp gradients are still present there. The subsequent trailing edge flow evolution (such as vortex shedding, the occasional propagation of the vortex upstream over the airfoil upper surface (Ref. 17), etc.) influences the other details aspects of the separated flow like reattachment, hysteresis loops, etc.

**4.2.2** Effect of Mach Number

Figure 7 presents interferograms for M = 0.3, 0.35, 0.4 and 0.45, obtained at k = 0.05 and $\alpha = 12.06$ deg. Fig. 7a at M = 0.3, shows a laminar separation bubble is about to break-down at this angle of attack. However, the effect is not detectable in the outer flow. Fig. 7b, at M = 0.35, shows the formation of vertical fringes from x/c = 0.04 to x/c = 0.15. It has been shown in Ref. 17 that this state represents the onset of dynamic stall and that the vortex is in its primitive stages of formation. The outer flow still is not affected by the major changes in the flow field close to the airfoil. At M = 0.4, (Fig. 7c) the dynamic stall vortex has fully developed and has convected over the airfoil surface; it should be pointed out that the imprint of the dynamic stall vortical region in compressible flow is not circular, but some what oval in shape. The outer edge of the vortex has reached about 30% chord; further downstream, the boundary layer has grown considerably in size. In contrast, Fig. 7d shows that at M = 0.45, the dynamic stall process has progressed to an extent where the vortex has already convected beyond x/c = 0.5. In fact, deep dynamic stall occurred for M = 0.45 and k = 0.05 at $\alpha = 14.2$ deg., but for M = 0.3, the corresponding angle was 15.9 deg. These quantitative results support the schlieren flow visualization discussed earlier. The corresponding global pressure distributions are shown in Fig. 7e to 7h. These were derived by using isentropic flow assumptions, even when a dynamic stall vortex was present, (it is believed that the errors introduced do not result in a different interpretation of the results at these Mach numbers). The dramatic influence of the vortical flow on the outer inviscid flow is clearly seen in Fig. 7g and Fig. 7h.

**4.2.3.** Delay of Stall Due to Unsteadiness

Figure 8 shows the peak suction pressure coefficient,

$C_{p_{min}}$ plotted as a function of angle of attack for M = 0.3, for steady flow (k = 0) and the unsteady flow cases of k = 0.05 and 0.1. The distribution for steady flow shows abrupt leading edge stall that is typical of NACA 0012 airfoil. The curves for the unsteady cases show a delay of stall from that of steady flow, which increases with k. This clearly points out that the airfoil develops less suction at comparable angles of attack and thus, the airfoil experiences a lesser adverse pressure gradient with increasing unsteadiness. The peak suction eventually reaches a value higher than that in steady flow, although the resultant adverse pressure gradient may not be much higher (see Fig. 10). It has been shown in Ref. 17 that for a transiently pitching airfoil, the suction pressure coefficient remains at the maximum value during the time when the dynamic stall vortex forms and organizes, and then drops as the vortex convects down the airfoil; the same result is seen for the oscillating airfoil also. The organization time seems to depend on the reduced frequency, since the amount of coherent vorticity introduced by the airfoil motion also depends on k. So, it can be expected that at higher reduced frequencies, the plateau seen in the $C_{p_{min}}$ distributions lengthens, leading to a longer stall delay; this effect can be seen in Fig. 8. The peak suction drops gradually once vortex convection begins.

Figure 9 compares the pressure distributions at M = 0.3 between the steady flow at $\alpha$ = 11.0 deg and unsteady flow at k = 0.05 at $\alpha$ = 10.0 deg. It is evident that the two compare very well, with only a slight deviation in the bubble region. The agreement indicates that the unsteady flow at a higher angle of attack is similar to steady flow at a lower angle of attack, prior to stall onset, pointing to a general lag of flow development in the unsteady flow. In this case for M = 0.3, and k = 0.05, this lag is one degree. The plateau seen in the distributions points to the existenc of a laminar separation bubble, since the pressure everywhere along the bubble is constant. The pressure rises normally after the bubble closes. The bubble forms over the airfoil since the Reynolds number (360,000 - 840,000) of the flow was in the transitional regime. The other small differences are within the one fringe the uncertainty of the PDI technique.

Figure 10 presents the pressure distributions for $0 \leq x/c \leq 0.05$ for k = 0, 0.05 and 0.1 at $\alpha$ = 10.0 deg. at M = 0.3. The plots show that the suction develops over an oscillating airfoil at a reduced rate as the frequency of oscillation is increased and in fact does not reach the steady state level at the angle compared. Past the suction peak, the pressure rises more slowly in the unsteady cases. This delay of the airfoil flow development, with corresponding delay in the development of the adverse pressure gradients can be seen to be one of the causes of dynamic stall delay that is observed. It should be noted that each symbol in Fig. 10 corresponds to a quantitative measure of the instantaneous pressure as obtained from the interferogram. This is the first set of data to show the lessening of the local adverse pressure gradient by unsteadiness in such detail and offers a reasonable explanation for the delay for stall.

#### 4.2.4. Formation of Multiple Shocks

For certain compressible flow conditions, (e.g. M = 0.45, k = 0.05, $\alpha = 10^{o}$) a shock or a series of shocks formed near the airfoil leading edge as shown in Fig. 11. The *lambda* shocks seen are characteristic of laminar flow behavior. Interestingly, the flow does not separate immediately once a shock forms. It seems to be able to withstand the local adverse pressure gradient caused by the shock for a small range of angle of attack before separating. A series of pictures for these experimental flow conditions showed that flow separation at the foot of the last shock eventually resulted in the dynamic stall vortex. At this time, the cause of the multiple shocks is still under investigation. It is believed that the first shock interacts with the laminar leading edge boundary layer introducing a waviness in the boundary layer thickness which seems to be sufficient for producing the expansion waves and compression waves necessary for the system to sustain itself during a small angle of attack sweep of the airfoil.

A map of the pressure coefficient distribution in the vicinity of the multiple shocks for the case shown above is presented in Fig. 12. The leading edge region has been magnified so that the flow variations due to the shocks can be analyzed. This unique quantitative evaluation of the *outer flow* was made possible by the fringe tracing/analysis algorithm developed specifically for this task. It is clear that the flow becomes supersonic near the surface and that a region of $M > 1$ (the sonic line corresponds to $C_p = -2.76$) which is significantly wider than previously thought exists in the flow. In this region, 5 shocks are present. The shocks terminate in the sonic line. The outer flow, however, is subsonic; this is one of the key differences in compressible dynamic stall flow that cannot be reproduced at low speeds. As the angle of attack is increased, the shock pattern changes since the interaction with the boundary layer changes. Eventually, a dynamic stall vortex appears at the foot of the last shock. The x/c location at which this happens is about 0.05 - 0.08, indicating that the dynamic stall vortex does not form at the leading edge. This figure attests to both the presence of the fine scale details in the flow as well as the ability of the measurement technique used in this research to capture them.

### 4.3. Role of Transition

As stated earlier, the dynamic stall vortex forms near the point where the separating shear layer undergoes transition. Thus, it can be expected that factors affecting transition also affect the processes of dynamic stall onset and vortex formation. Applicability of low Reynolds number testing methods and test data to model rotors and eventually to flight Reynolds numbers thus becomes a formidable challenge and suffers from several limitations. Whereas this situation is not new, it is nevertheless a major issue in model rotor testing, since the process of flow separation is particularly sensitive to the state of the boundary layer. A standard approach to simulate high Reynolds number

results in the laboratory is to conduct tests by tripping the airfoil boundary layer with the intent that the flow subsequently develops as a fully turbulent flow. It is important to recognize that despite the vast number of previous experimental studies on tripping in steady flow and the recommendations on the right kind of trips that have resulted, these schemes are not directly applicable to dynamic stall flow; and the use of steady flow tripping schemes for dynamic stall flow studies has not been satisfactory.

#### 4.3.1 Description of the Trips

The airfoil boundary layer at the vortex formation location on the present model was $O(50\mu m)$; hence, the trip height that was needed was much smaller than this. Also, the trip used could radically change the stall behavior of the airfoil, Ref. 7. Thus, it was imperative that tests be conducted with a series of trips and that selection be based on which trip provided "turbulent" flow-like information. As part of this study, five different trips were studied in the CDSF. Randomly distributed roughness elements (aluminum oxide particles or grit) were glued on to the airfoil surface by a thin lacquer or adhesive, depending upon the trip material. The trip height ranged from $170\mu m$ to about the height of the boundary layer, $\approx 50\ \mu m$. The length was either 3% chord, starting at 1% chord location (near the leading edge) to 4% chord; or from stagnation point on the lower surface to 4% chord point on the upper surface. PDI data was obtained for the flow over an oscillating with the different trips installed, at several Mach numbers and reduced frequencies. The trips were evaluated based on the criteria of elimination of the laminar separation bubble, delay of dynamic stall and the production of higher suction levels than the untripped airfoil. The trip that satisfied these conditions was accepted as the "right" trip. This optimum trip was made from 22-$36\mu m$ aluminium oxide particles deposited over a thin lacquer coating installed with a total height of about $43\mu m$ from $0.005 \leq x/c \leq 0.03$.

#### 4.3.2 Qualitative Analysis

Figure 13a and 13b compare interferograms over the airfoil with and without the optimum trip at M = 0.3 and k = 0.05 and $\alpha$ = 10.0deg. The presence of the laminar bubble (described in Sec. 4.2.2, Fig. 6) can be clearly found in Fig. 13a by studying the fringe pattern. In Fig. 13b, the fringe very near the airfoil leading edge shows a closed loop pattern, which corresponds to a well defined suction peak. The fringes slightly downstream of the suction peak meet the upper surface over a small length of the airfoil region rather than near a point as seen in Fig. 13a. This fringe pattern indicates the absence of the bubble; the corresponding pressure distributions confirmed this interpretation (Ref. 7). Fig. 13c shows the flow field at $\alpha$ = 13.99deg. when the dynamic stall vortex has fully formed and has convected past the x/c = 0.25 point for the untripped airfoil, whereas in Fig. 13d, at the same angle of attack, the vertical fringes which precede the dynamic stall vortex have just appeared, pointing very definitely to delay of stall that was achieved due to the presence of the trip, (it is worth pointing that if improper trips were used, the stall process could even be accelerated, as was demonstrated in Ref. 18).

#### 4.3.3. Quantitative Analysis

Figure 14 presents the variation of the airfoil peak suction in the presence of the trip at M = 0.45 and k = 0.05. The significantly increased suction levels are proof that the airfoil was tripped successfully and a flow more representative of turbulent flow dynamic stall was achieved in the wind tunnel. It is interesting to note that the $C_{p_{min}}$ values for both the untripped and tripped airfoil exceed the critical value of -2.76; thus, the flow in both cases becomes supersonic. The larger $C_p$ values of the tripped airfoil flow suggest that the local Mach numbers in this flow are higher. It is interesting to note that despite the larger Mach number, the shock system that results over the airfoil is much less dramatic (see Fig. 15 compared to Fig. 12), once again attributable to the turbulent flow over it. The corresponding pressure distribution obtained from a PDI image is shown in Fig. 15 for M = 0.45, k = 0.05 and $\alpha$ = 10.0deg. In comparison with Fig. 12, (multiple shocks flow field over the untripped airfoil at the same conditions) it is seen that the local $C_p$ values are higher and that the sonic line is much broader. Its shape is also different, with a bulging front and a longer tail extending to x/c = 0.15. Despite the larger Mach numbers, only two shocks (represented by the dotted lines nearly normal to the surface) are seen in it. Further, there is no flow separation seen in this case. This pair of figures graphically demonstrates the importance of proper tripping of the boundary layer, especially in unsteady compressible flow. It is interesting that there is qualitative similarity of this result to the turbulent computational dynamic stall studies of Ref. 19 and 20.

### 4.4. Role of Adverse Pressure Gradient

Analysis of the adverse pressure gradient near the untripped airfoil leading edge at M = 0.3 showed that dynamic stall was caused by the *failure of the laminar shear layer to reattach* (Ref. 18) due to the levels of this gradient. At higher Mach numbers dynamic stall occurred either from the above reason or from a shock-induced separation. It has been shown in Ref. 18 that dynamic stall is initiated over a transiently pitching airfoil when the leading edge adverse pressure gradient $\left(\frac{dC_p}{d(x/c)}\right)$ reaches a critical value that depends upon Mach number and pitch rate. Fig. 16 (Ref. 18) shows that the critical value of the adverse pressure gradient decreases with increasing Mach number, once again indicating the strong influence of compressibility on the process. It appears that compressibility weakens the ability of the boundary layer to withstand the adverse pressure gradient, even though the adverse pressure gradient value is smaller. Increasing the pitch rate seems to enable the boundary layer to withstand higher levels of adverse pressure gradients,(Fig. 10, Ref. 18). The results seem to be true for both the untripped and tripped airfoil, leading to the conclusion that unsteadiness introduces certain changes to the leading edge vorticity layer and makes it behave differently.

Figure 17 presents the adverse pressure gradient development over the oscillating airfoil at M = 0.3 at k = 0.05. For the untripped airfoil, the pressure gradient immediately following the suction peak is plotted. It was found that the value of the pressure gradient at the formation of the laminar separation bubble is about 40, at an angle of attack of about 7 deg. Dynamic stall is seen to occur at a pressure gradient of 125 at $\alpha$ = 12.5deg. As the dynamic stall vortex begins to convect, the pressure gradient drops. In case of the tripped airfoil, the dynamic stall process begins at $\alpha$ = 13.5deg., when the pressure gradient is about 150. Thus, there is a slight delay of stall, attributable to an improvement in the ability of the boundary layer to withstand the forces inducing flow separation. The trends at other reduced frequencies were nearly the same, although at times the pressure gradients at the angle of attack of dynamic stall vortex formation were slightly less for the tripped airfoil when compared to the untripped flow. But, the values were *always* higher than that at which the laminar separation bubble formed in the untripped flow. Some of the differences seen can be attributed to the noise inherent in the process of numerical differentiation of the pressure distribution to recover the pressure gradient information. Also, any trip, however small it is, still increases the momentum thickness of the boundary layer and hence, introduces additional drag, which has the equivalent effect of reducing the total adverse pressure gradient that can be attained before stall occurs. This points to the difficulty of conducting laboratory tests by tripping to simulate the higher Reynolds number flow, a fact of critical importance to model rotor testing.

## 5. CONCLUSIONS

A review of results from an ongoing study of the effects of compressibility on dynamic stall of oscillating airfoils has been presented. A unique compressible dynamic stall facility was designed and developed for this purpose. The flow was studied using stroboscopic schlieren and stroboscopic point diffraction interferometry(PDI) techniques. The latter was developed for use in unsteady separated flows to provide a quantitative description of the instantaneous surface and global pressure distributions of the flow. The experimental conditions were chosen to be directly relevant to that encountered by the retreating blade of a helicopter model rotor. The results show that the process of dynamic stall vortex formation occurs rapidly in a very small (half-a-degree) angle of attack range. Compressibility effects become critical at a free stream Mach number of 0.3. Compressibility promotes dynamic stall onset by decreasing the angle of attack at which the flow separates with increase in Mach number. The strongly compressible local flow can produce multiple shocks in the leading edge region, and at times can also induce flow separation leading to dynamic stall. Increasing the reduced frequency delays stall onset, even under compressible conditions. As much as two degrees of stall onset delay was observed at M = 0.3 when compared to steady flow. The PDI results also revealed that dynamic stall occurred as the laminar separation bubble that formed over the airfoil broke down. Evidence points to the failure of the laminar shear layer to reattach as the cause of stall onset. This premature stall at higher Mach numbers could be attributed to the inability of the compressible boundary layer to withstand the adverse pressure gradient in the flow. Increasing unsteadiness has a beneficial effect in this regard, even in compressible flow. Tests conducted to simulate higher Reynolds number flow situations by tripping the leading edge boundary layer have revealed some of the issues and concerns of tripping leading-edge-stalling flows.

The various fluid flow physics issues that have been uncovered by this investigation include formation of multiple shocks, effects of leading edge pressure gradient in unsteady flow separation as affected by the degree of unsteadiness, the delay of the leading edge pressure development with increase in pitch rate, and the effects of boundary layer transition. The quantitative flow field data base that has been developed will be of significant value to researchers involved in flow modelling and in validating CFD codes developed to represent this complex and challenging flow phenomenon.

## ACKNOWLEDGEMENTS

The project was supported by ARO-MIPR-114-91, 132-92, and 125-93 to the Naval Postgraduate School and was monitored by Dr. T.L. Doligalski. Additional support was received from the U.S. AFOSR, which was monitored by Maj. D.B. Fant. The work was carried out in the Fluid Mechanics Laboratory Branch of NASA Ames Research Center. The steady encouragement of Dr. S.S. Davis, Chief, FML Branch, the able assistance of Dr. M.C. Wilder while performing the experiments, the support of Mr. J.D. Loomis in the conduct of experiments and the interferogram image processing support of Ms. S.Nado are greatly appreciated.

## 6. REFERENCES

1. W.J., McAlister, K.W., Carr, L.W., Pucci, S.L., Lambert, O. and Indergrand, R.F., "Dynamic Stall on Advanced Airfoil Sections," AHS Journal, *26*,3, July 1981, pp. 40-50.
2. Carr, L.W., "Progress in Analysis and Prediction of Dynamic Stall," J. Aircraft, *25*,1, Jan. 1988, pp. 6-17.
3. McCroskey, W.J., "The Phenomenon of Dynamic Stall," NASA TM 81264, March 1981.
4. Gostelow, J.P., Blunden, A.R. and Walker, G.J., "Effects of Free-Stream Turbulence and Adverse Pressure Gradients on Boundary Layer Transition", *ASME Paper No. 92-GT-380*, IGTE, Cologne, Germany, June 1-4, 1992.
5. Tan, C.M., and Carr, L.W., A Report on the 1992 AFDD International Dynamic Stall Workshop on "Correlation of Dynamic Stall Models with 3-D Dynamic Stall Data" NASA TM in preparation, 1994.
6. Lorber, P.F., Strauer, R.C., Haas, R.J., Anderson, T.J., Torok, M.S. and Kohlhepp, F.W., "Techniques for Comprehensive Measurement of Model Helicopter Rotor Aerodynamics", *AHS Forum 50*, Washington, D.C., May 11-14, 1994.

7. Chandrasekhara, M.S., Wilder, M.C. and Carr, L.W., "Boundary Layer Tripping Studies of Compressible Dynamic Stall Flow", *AIAA Paper No. 94-2340*, $25^{th}$ Fluid Dynamics Conference, Colorado Springs, Co, June 20-23, 1994.
8. Carr, L.W., McAlister, K.W. and McCroskey, W.J., "Analysis of Development of Dynamic Stall Based on Oscillating Airfoil Experiments", NASA TN D-8382, 1977.
9. Liiva, J., "Unsteady Aerodynamic and Stall Effects on Helicopter Rotor Blade Airfoil Sections", J.Aircraft, *5*,1, Jan-Feb. 1969, pp. 46-51.
10. Carr, L.W. and Chandrasekhara, M.S., "Design and Development of a Compressible Dynamic Stall Facility", J. Aircraft, *29*,3, May-June 1992, pp. 314-318.
11. Brock, N., Chandrasekhara, M.S. and Carr, L.W., "A Real Time Interferometry System for Unsteady Flow Measurements", *in* "ICIASF'91 RECORD", IEEE Publication 91CH3028-8, pp. 423-430.
12. Chandrasekhara, M.S. and Carr, L.W. "Flow Visualization Studies of the Mach Number Effects on the Dynamic Stall of Oscillating Airfoils", J. Aircraft, *27*,6, June 1990, pp. 516-522.
13. Platzer, M.F., Chandrasekhara, M.S., Ekaterinaris, J.A, and Carr, L.W., "Dynamic Airfoil Stall Investigations", *in* "Proc. $5^{th}$ Symposium on Numerical and Physical Aspects of Aerodynamic Flows", Long Beach, CA, January 13-15, 1992.
14. Chandrasekhara, M.S. and Brydges, B.E., "Amplitude Effects on Dynamic Stall of an Oscillating Airfoil", *AIAA Paper 90-0575*, $28^{th}$ Aerospace Sciences Meeting, Reno, NV, January 1990.
15. Carr, L.W., Chandrasekhara, M.S., Ahmed, S. , and Brock, N.J.,"A Study of Dynamic Stall Using Real Time Interferometry," *AIAA Paper 91-0007*, To appear in J. Aircraft.
16. Carr, L.W., Chandrasekhara, M.S. and Brock, N.J., "A Quantitative Visual Study of Unsteady Compressible Flow on an Oscillating Airfoil", *AIAA Paper 91-1683*, To appear in J. Aircraft.
17. Chandrasekhara, M.S., Carr, L.W. and Wilder, M.C., "Interferometric Investigations of Compressible Dynamic Stall Over a Transiently Pitching Airfoil", AIAA Journal, *32*, 3, Mar. 1994, pp. 586-593.
18. Wilder, M.C., Chandrasekhara, M.S., and Carr, L.W., "Transition Effects on the Compressible Dynamic Stall of Transiently Pitching Airfoil", *AIAA Paper No. 93-2978*, $24^{th}$ Fluid Dynamics Conference, Orlando, FL, July 6 -9, 1993.
19. Visbal, M.R., "Effect of Compressibility on Dynamic Stall of a Pitching Airfoil", *AIAA Paper 88-0132*, Jan. 1988.
20. Ekaterinaris, J.A., "Compressible Studies of Dynamic Stall", *AIAA Paper 89-0024*, Jan., 1989.


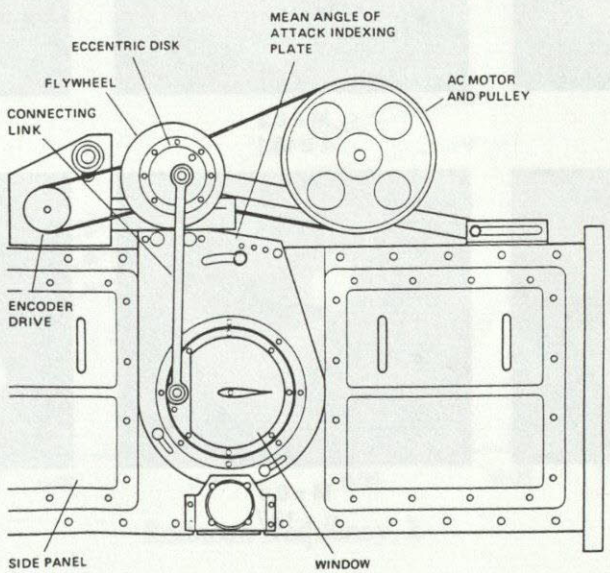


Fig. 1. Schematic of the Compressible Dynamic Stall Facility

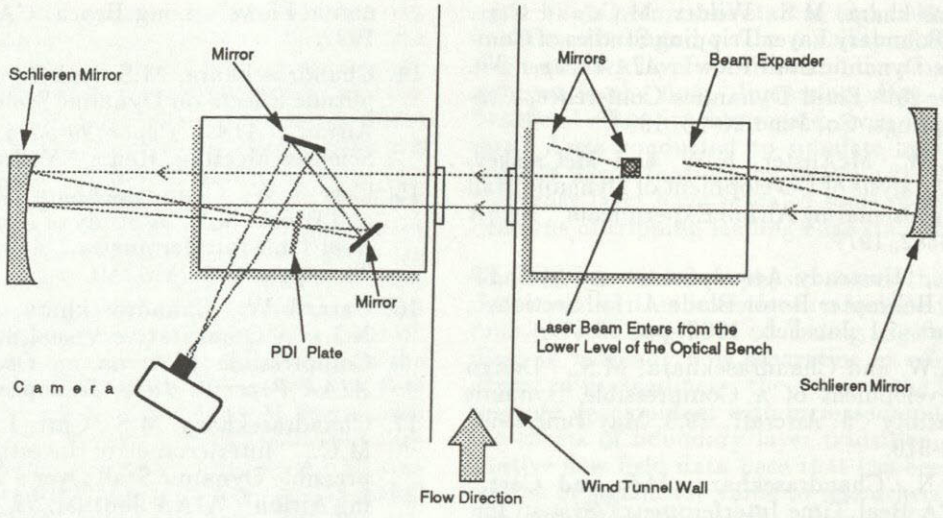


Fig. 2. Schematic of the Point Diffraction Interferometry System.

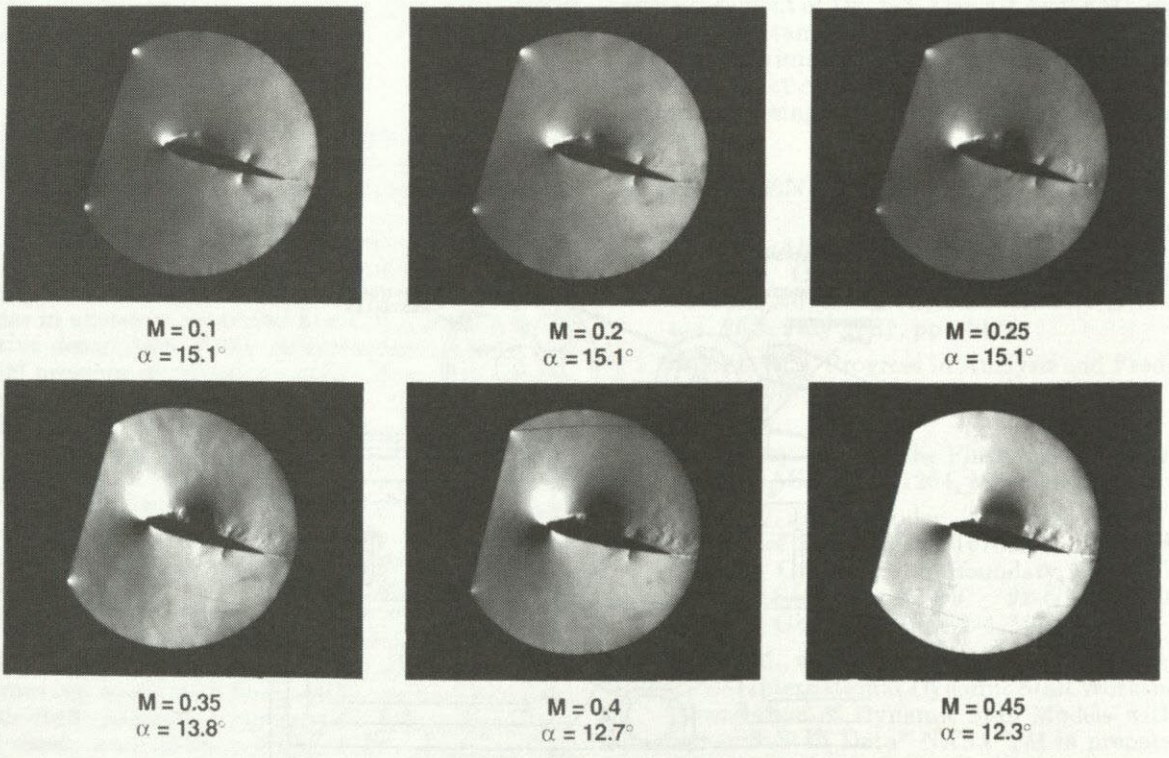


Fig. 3. Effect of Compressibility on Dynamic Stall of an Oscillating Airfoil; k = 0.05.

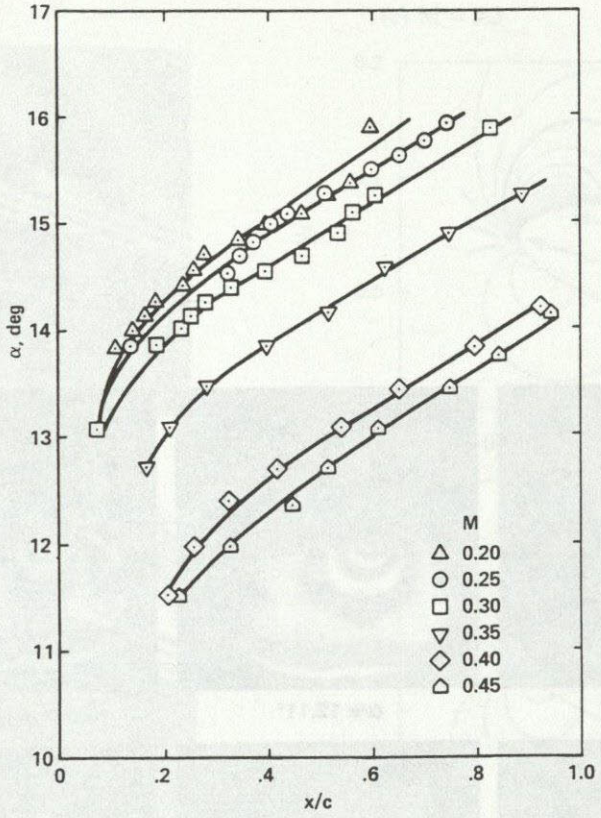


Fig. 4. Quantitative Effects of Mach Number on Dynamic Stall Process; k = 0.05.

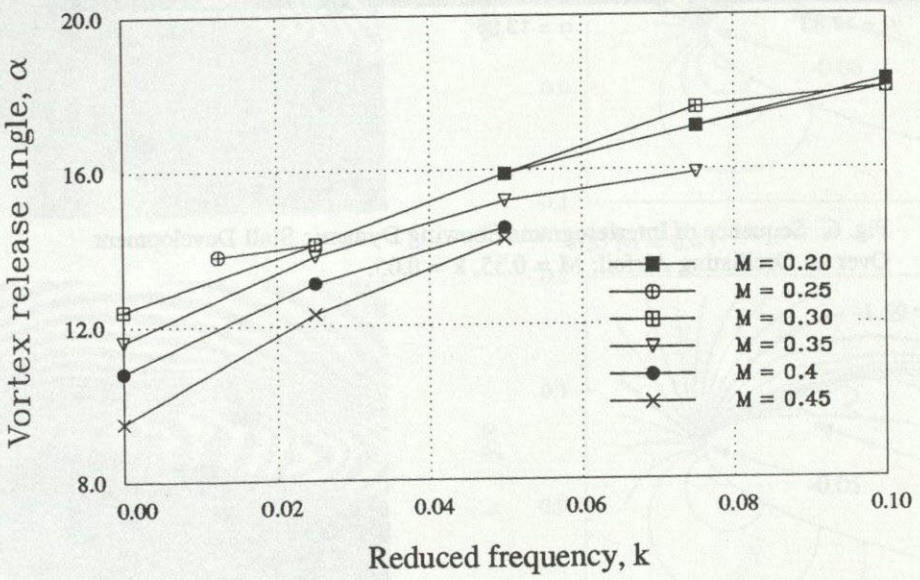


Fig. 5. Quantitative Effects of Reduced Frequency on Dynamic Stall Process.

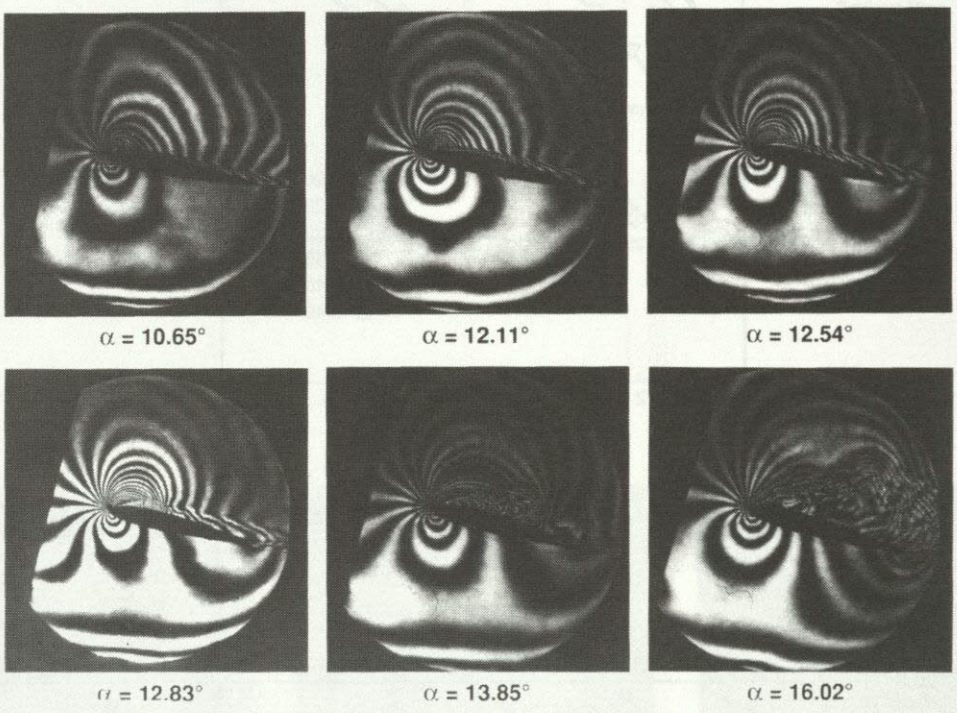


Fig. 6. Sequence of Interferograms Showing Dynamic Stall Development Over an Oscillating Airfoil; M = 0.35, k = 0.05.

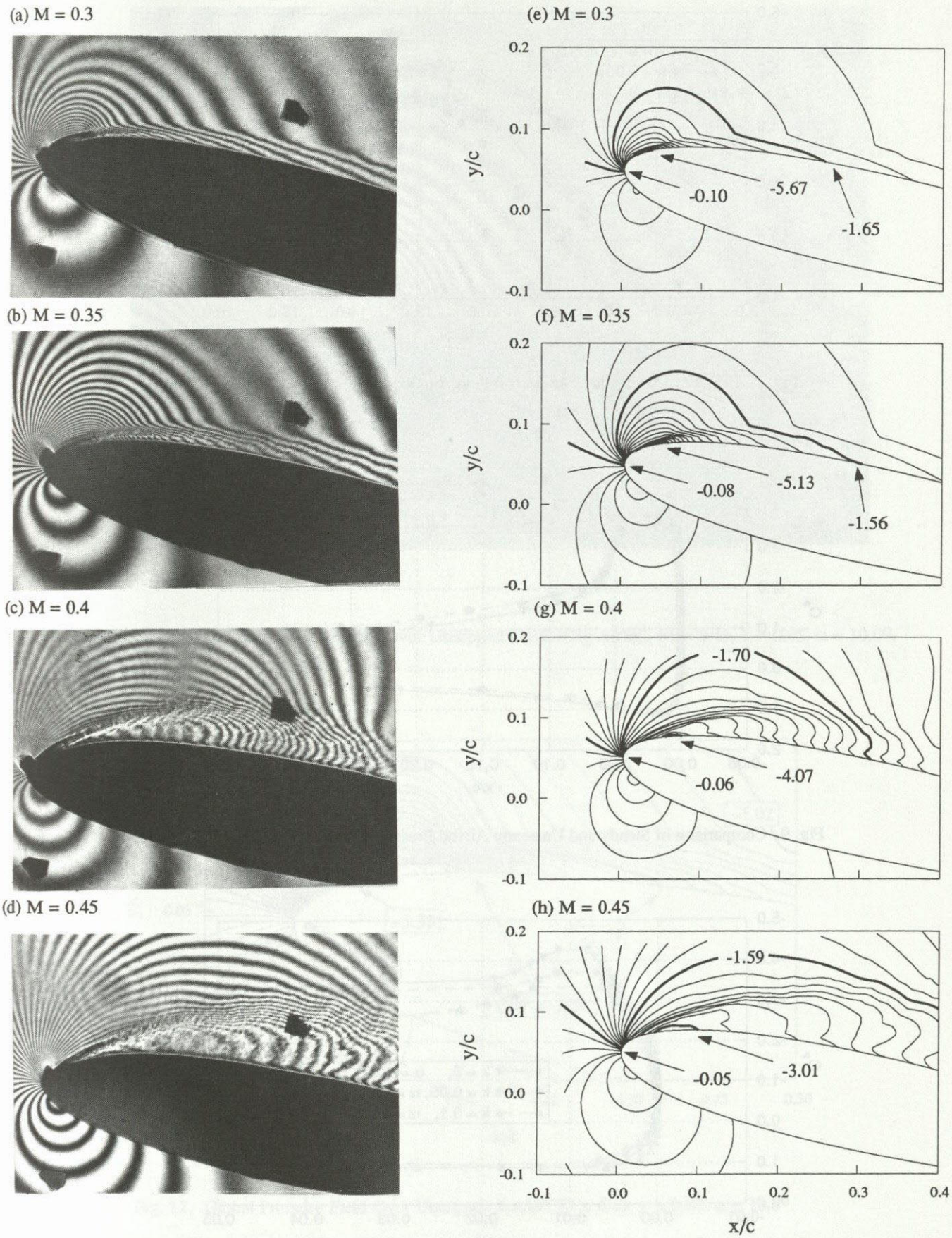


Fig. 7. Effect of Compressibility on Dynamic Stall; (a–d) PDI Images; (e–h) Global Pressure Fields.

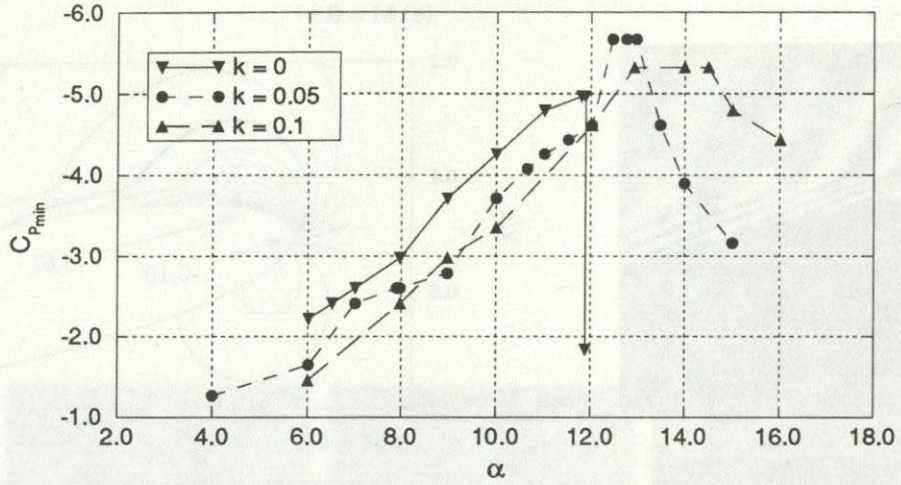


Fig. 8. Effect of Unsteadiness on Airfoil Peak Suction Development; M = 0.3.

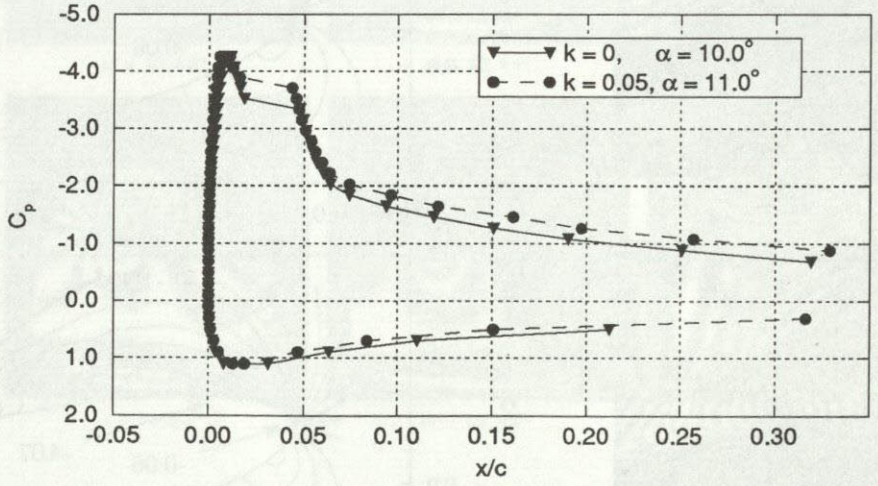


Fig. 9. Comparison of Steady and Unsteady Airfoil Pressure Distributions; M = 0.3.

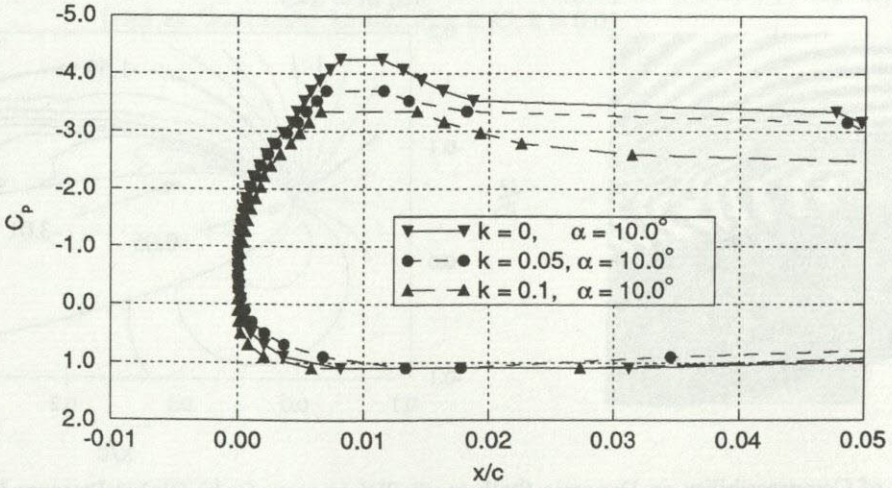


Fig. 10. Effect of Unsteadiness on Airfoil Leading-Edge Pressure Distribution; M = 0.3.

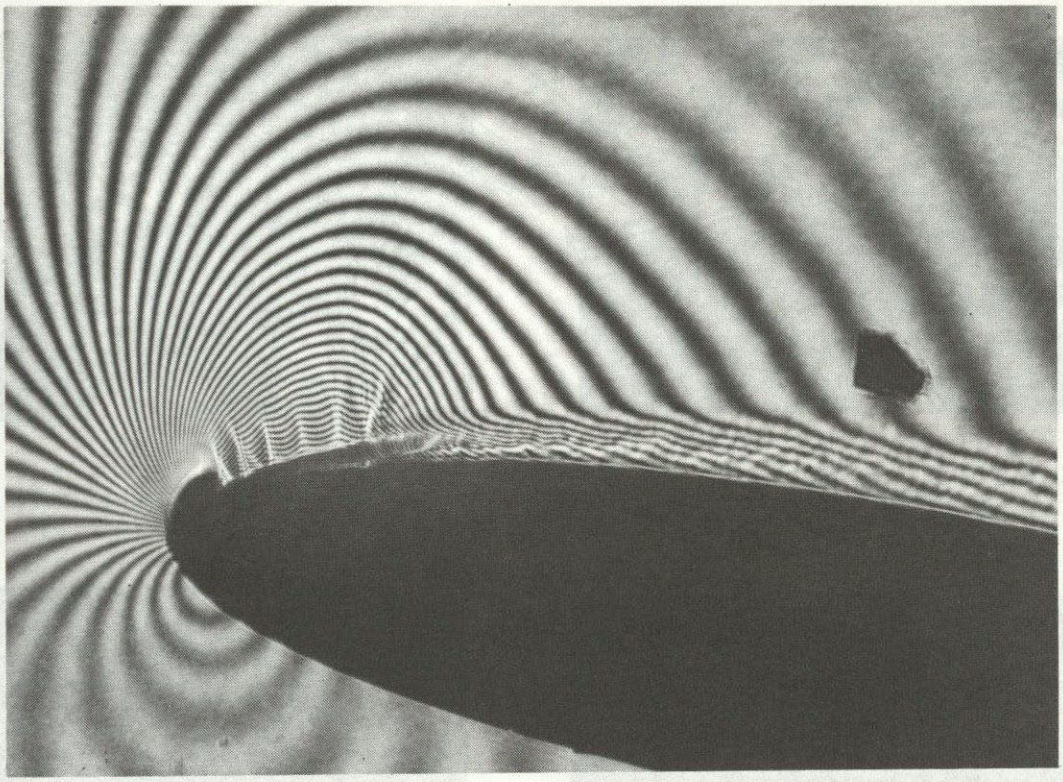

Fig. 11. PDI Image of Multiple Shocks Over Untripped Oscillating Airfoil; M = 0.45, k = 0.05, $\alpha = 10.0^{o}$.

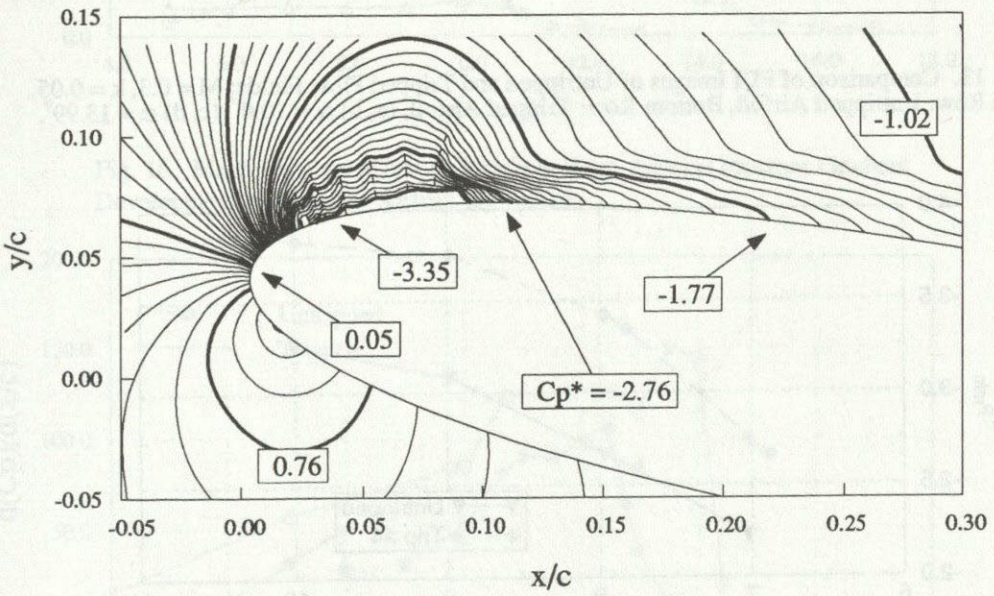


Fig. 12. Global Pressure Field Over Untripped Airfoil; M = 0.45, k = 0.05, $\alpha = 10.0^{o}$.

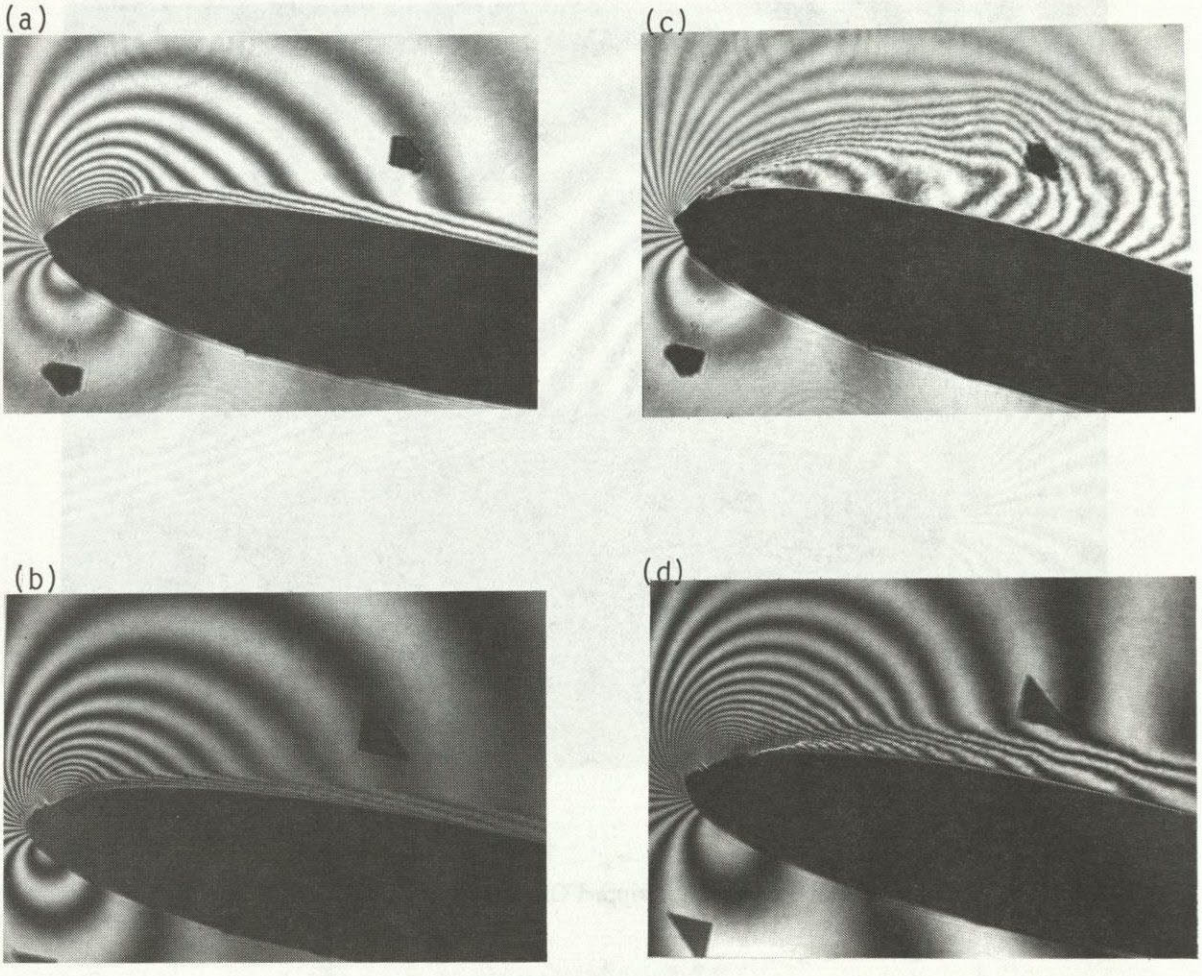


Fig. 13. Comparison of PDI Images of Untripped and Tripped Flow Fields; M = 0.3, k = 0.05. Top Row: Untripped Airfoil, Bottom Row: Tripped Airfoil, (a, b) $\alpha = 10.0^{\circ}$, (c, d) $\alpha = 13.99^{\circ}$.

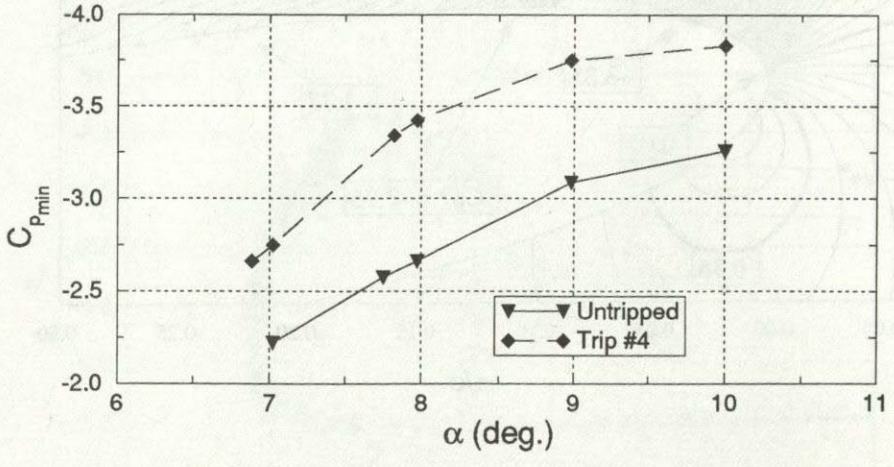


Fig. 14. Effect of Tripping on Airfoil Peak Suction Development; M = 0.45, k = 0.05.

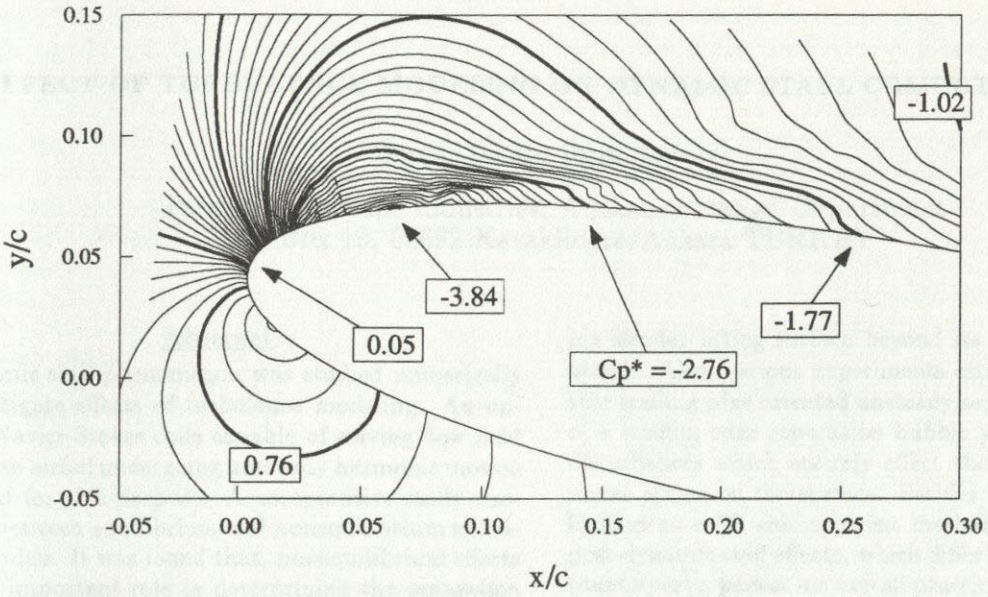


Fig. 15. Global Pressure Coefficent Field Over Tripped Airfoil; M = 0.45, k = 0.05, $\alpha = 10.0^{o}$.

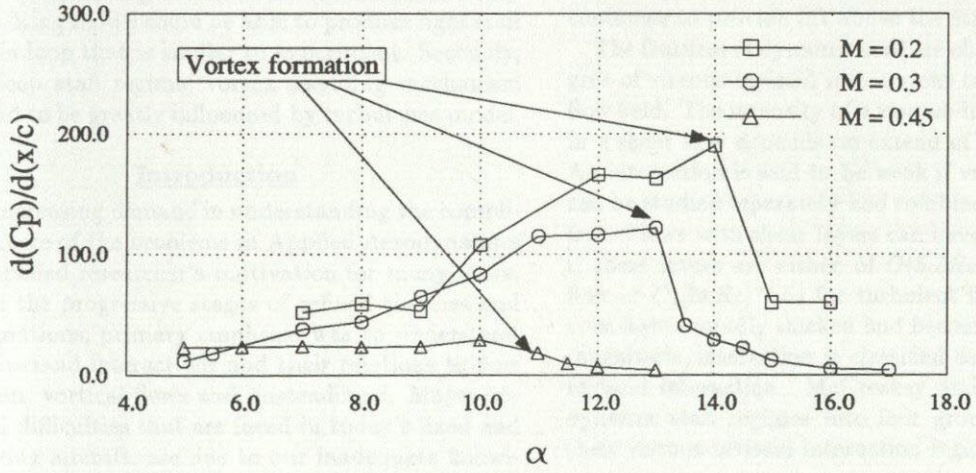


Fig. 16. Mach Number Effect on Leading–Edge Adverse Pressure Gradient Development on Tripped Airfoil; $\alpha^{+} = 0.03$.

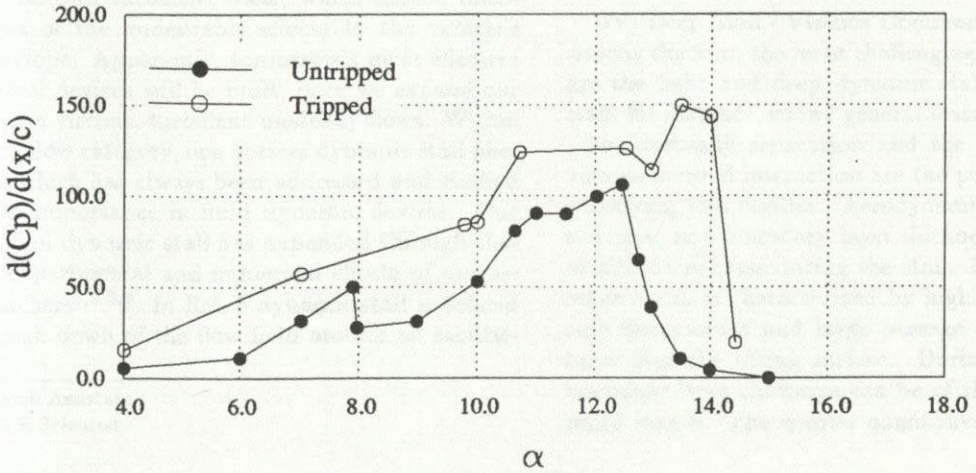


Fig. 17. Leading–Edge Adverse Pressure Gradient Development; M = 0.3, k = 0.05.